Surface Clutter Due to Antenna Sidelobes for Spaceborne Atmospheric Radar

Stephen L. Durden, *Senior Member, IEEE*, Eastwood Im, *Senior Member, IEEE*, Fuk K. Li, *Fellow, IEEE*, Ralph Girard, and Kyung S. Pak

***Abstract*—A spaceborne radar for atmospheric observation must be able to detect atmospheric backscatter in the presence of clutter from the surface, due to antenna sidelobes. Such clutter can come from the same pulse as that observing the atmosphere if the radar antenna is pointed off-nadir. However, pulses both prior and subsequent to the pulse observing the atmosphere can also contribute to clutter, and surface clutter can be a problem even for nadir-looking radars. Here, the problem is analyzed by deriving a method for computing clutter which includes effects of all contributing transmit pulses, Doppler shifting, finite receiver bandwidth, and curved earth's surface. The results are applied to analysis of existing radars and design of future radar systems.**

***Index Terms*—Clouds, clutter, precipitation, radar, sidelobes.**

I. Introduction

A SPACEBORNE atmospheric radar must be well designed to provide a detectable signal from distant and often weak atmospheric targets, such as clouds or precipitation. In addition to minimizing thermal noise, it must also be designed to minimize interfering return, or clutter, coming from the earth's surface through the antenna sidelobes. Calculation of surface clutter has been addressed in [1]–[3], with application to cross-track scanning spaceborne precipitation radars. Those works addressed the case of interference from the same pulse as that illuminating the atmosphere. Here, we extend this work to include effects of all contributing transmit pulses, Doppler shifting, finite receiver bandwidth, and spherical earth. The results are first demonstrated using data from existing radars and then applied to the design of future radar systems.

II. Approach for Signal-to-Clutter Calculation

The geometry of a spaceborne radar observation of the atmosphere is shown in Fig. 1. The radar antenna's main beam is assumed to be scanned in the cross-track dimension, and, for our analysis, the main beam may be pointed at nadir or off-nadir to either side of the satellite track with scan angle α. While the main beam illuminates the atmospheric target, antenna sidelobes illuminate the surface. Our concern is the calculation of the ratio of atmospheric return (signal) to simultaneous surface return (clutter). The atmospheric return power P_a is calculated by the Probert–Jones equation [4]

$$P_a(r_a) = \frac{P_t \lambda^2 G^2 \theta_1^2 \Delta \eta L_a}{512\pi^2 \ln 2 r_a^2} \tag{1}$$

where

- P_t transmitter power;
- λ wavelength;
- G antenna gain;
- θ_1 antenna half-power beamwidth;
- Δ range resolution;
- η reflectivity;
- L_a atmospheric attenuation;
- r_a range to the atmospheric target.

In this equation and our subsequent derivations, we assume that the pulse shape is nearly constant over the resolution Δ and zero outside. Equation (1) also assumes a Gaussian-shaped antenna pattern over the main beam.

In addition to the signal from the atmosphere, the radar will simultaneously receive echoes from all targets which differ in range by $nc/2\text{PRF}$, where n is an integer, c is the speed of light, and PRF is the pulse repetition frequency. This is just the range ambiguity problem common to all pulsed radars [5], [6]. The number n corresponds to the pulse number relative to the pulse being received from the atmospheric target, with positive n denoting previous pulses and negative n denoting subsequent pulses, and $n = 0$ denoting the pulse being received from the atmospheric target. The surface return P_s for a particular n is given by the following expression [3]:

$$P_s(r_s) = \frac{P_t \lambda^2 G^2}{64\pi^3} \int_S \frac{g^2 \sigma^o L_s}{r_s^4}\, dS \tag{2}$$

where

- S surface illuminated by the pulse;
- σ^o normalized radar cross section of the surface;
- g antenna pattern;
- L_s atmospheric path attenuation to the surface.

The range to the surface r_s is equal to $r_a + nc/2\text{PRF}$.

As discussed in [1]–[3], the surface clutter through sidelobes for a given n is due to an annulus on the earth's surface. This assumes a rectangular pulse, as was also assumed in the derivation of (1). For large n, the clutter can come from annuli with large radii, so the effects of surface curvature must be included, as shown in Fig. 1. For a given n, and hence r_s, the integral in (2), denoted by I, can be evaluated by writing it in spherical coordinates, with origin at the earth's center, azimuth angle ϕ, and

Manuscript received April 7, 2000; revised March 6, 2001. This work was supported by the Jet Propulsion Laboratory, California Institute of Technology, under contract with NASA, and by the Canadian Space Agency.

S. L. Durden, E. Im, F. K. Li, and K. S. Pak are with the Jet Propulsion Laboratory, California Institute of Technology, Pasadena, CA 91109 USA.

R. Girard is with the Canadian Space Agency, St. Hubert, QC, Canada.

Publisher Item Identifier S 0196-2892(01)07623-9.

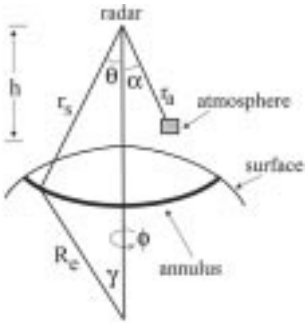

Fig. 1. Coordinate system for clutter calculations, illustrating look angle θ from nadir to surface clutter, scan angle α from nadir to atmospheric target, elevation angle γ between earth radii pointing at radar and pointing at source of surface clutter, and azimuth angle ϕ.

elevation angle γ, defined as the angle subtended by the earth's surface from nadir to the annulus. We find

$$I = R_e^2 \int_0^{2\pi} \int_{\gamma_1}^{\gamma_2} \frac{g^2 \sigma^o L_s}{r_s^4} \sin\gamma \, d\gamma \, d\phi \tag{3}$$

where γ_1 is the angle to the inner edge of the annulus, and γ_2 is the angle to the outer edge of the annulus. The earth radius R_e is constant and has been brought outside the integral. We assume that g^2, σ^o, L_s, and r_s are essentially constant over the width of the annulus, and we bring these quantities outside the γ integral. This leaves the integral of $\sin\gamma \, d\gamma$, which is just $\cos\gamma_1 - \cos\gamma_2$. Using the law of cosines to find both $\cos\gamma_2$ and $\cos\gamma_1$, we find that

$$\cos\gamma_1 - \cos\gamma_2 = \frac{(r_2^2 - r_1^2)}{2R_e(R_e + h)} \tag{4}$$

where

$r_1 \equiv r_s - \Delta/2$ distance to the inner annulus edge;
$r_2 \equiv r_s + \Delta/2$ distance to the outer annulus edge;
h radar altitude.

These results can be combined to provide the following expression for the received power from the surface:

$$P_s(r_s) = \frac{P_t \lambda^2 G^2}{64\pi^3} \frac{R_e}{R_e + h} \frac{(r_2^2 - r_1^2)}{2r_s^4} \int_0^{2\pi} g^2(\theta, \phi) \sigma^o(\theta, \phi) \cdot L_s(\theta, \phi) \, d\phi. \tag{5}$$

Here, r_s, r_1, and r_2 have been brought outside the ϕ integral since they are independent of ϕ. We allow g^2, σ^o, and L_s to be functions of ϕ and so include them inside the ϕ integral. The angle θ is the look angle from the spacecraft to the annulus center, also shown in Fig. 1. When the surface area being illuminated is indeed an annulus, the expression $(r_2^2 - r_1^2)$ reduces to $2r_s\Delta$. However, near nadir the annulus can become a circle. In this case r_1 is less than the altitude h and should be replaced by h. This case is handled similarly in [1]–[3].

The discussion up to this point has neglected the effect of receiver bandwidth. As shown in [7], finite receiver bandwidth produces a loss that must be included in the analysis of weather radar performance. For the case at hand, there can be a loss in both signal power and clutter power. If the signal and clutter both had the same Doppler shift, the losses would be approximately equal and could be ignored when finding the ratio of signal to clutter, since they would cancel. However, the Doppler shifts for signal and clutter are not equal. To incorporate the effects of Doppler shifting and finite receiver bandwidth, we derive a weighting function with value between zero and unity, reaching unity for zero Doppler. To do this, we consider the receiver output voltage spectrum $V_o(f)$, which is equal to $H(f)V(f - f_d)$. Here, $H(f)$ is the receiver transfer function, $V(f - f_d)$ is the Doppler shifted input voltage spectrum, and f_d is the Doppler shift. The output energy is found by integrating the magnitude squared of the voltage over frequency. Following normalization by the receiver output for zero Doppler, we obtain the weighting function w as

$$w(f_d) = \frac{\int |H(f)V(f - f_d)|^2 \, df}{\int |H(f)V(f)|^2 df}. \tag{6}$$

For the rectangular pulse shape assumed in this paper, $V(f)$ is a sinc function. The Doppler frequency f_d is $2\hat{k} \cdot \vec{v}/\lambda$, where $\vec{v}$ is the velocity vector of the scatterer (atmosphere or surface) relative to the radar, and $\hat{k}$ is the unit vector from the radar in the direction of the scatterer. We denote the weighting due to Doppler shifting for the atmosphere by w_a and that for the surface by w_s. Because the Doppler shift varies with ϕ over an annulus, w_s must be included inside the integral in (5).

An explicit formula for the signal-to-clutter ratio (SCR), defined as the ratio of received atmospheric power to received surface power, can be found by combining (1) and (5)

$$\text{SCR} = \frac{\pi \theta_1^2 \eta L_a \Delta (R_e + h) w_a}{4 \ln 2 r_a^2 R_e \Sigma} \tag{7}$$

where

$$\Sigma \equiv \sum_n \frac{(r_2^2 - r_1^2)}{r_s^4} \int_0^{2\pi} w_s(f_d(\theta_n, \phi)) g^2(\theta_n, \phi) \cdot \sigma^o(\theta_n, \phi) L_s(\theta_n, \phi) \, d\phi.$$

Here, the summation over n includes all contributing annuli, or pulses. For each n, the angle θ_n to the corresponding annulus is computed as

$$\theta_n = \arccos \frac{(h + R_e)^2 + r_s^2 - R_e^2}{2r_s(h + R_e)} \tag{8}$$

where n determines r_s. For a flat surface there is no limit on the maximum positive n, since we can have annuli extending to infinity. For a spherical earth model, however, the maximum angle at which surface return can be received is

$$\theta_{\max} = \arcsin R_e/(R_e + h). \tag{9}$$

The existence of this maximum angle and, hence, maximum range limits n to a maximum positive value. The minimum angle at which clutter return can occur is zero, or nadir, setting a lower bound on n. For nadir-looking radars, the minimum value of n is zero. In other words when looking at nadir the surface return due to subsequent pulses always occurs later than the atmospheric return for the current pulse. For scanning radars this is no longer true, and n can become negative. In this case surface clutter at

nadir can be due to pulses subsequent to the pulse illuminating the atmosphere.

Equation (7) can be solved for η_m, the minimum detectable reflectivity, defined as that reflectivity which yields an SCR of unity (0 dB)

$$\eta_m = \frac{4 \ln 2 r_a^2 R_e \Sigma}{\pi \theta_1^2 L_a \Delta (R_e + h) w_a}. \tag{10}$$

The minimum detectable reflectivity factor, $Z_m \equiv \lambda^4 \eta_m / \pi^5 |K|^2$, can then be found. K is the dielectric constant factor for the atmospheric target [5].

Equation (10) is a general expression for the minimum detectable reflectivity due to clutter. For computations we need explicit formulas for the antenna pattern g, the surface cross section σ^o, the atmospheric attenuations L_a and L_s, and the receiver filter shape. We also need to determine the scatterer velocity $\vec{v}$. The antenna pattern is modeled as a Gaussian shaped mainbeam with sidelobes which are either flat or fall off as a monotonically decreasing function. In the log domain we have

$$g(\theta') = \begin{cases} -12(\theta'/\theta_1)^2 & \text{if } \theta' < \theta_s \\ -g_s - c(\theta' - \theta_s)^{1/2} & \text{otherwise} \end{cases} \tag{11}$$

where

$g(\theta')$	pattern in decibels;
g_s	level at which the mainbeam and sidelobe levels are equal;
$\theta_s = \theta_1 (g_s/12)^{1/2}$	corresponding angle;
C	constant.

θ' is the antenna elevation coordinate relative to the antenna boresight, and a more general antenna (i.e., a pattern that is not circularly symmetric) would use (θ', ϕ'). This is in contrast with (θ, ϕ) used above, which are in the radar global coordinates. The two coordinate systems are related by a rotation angle α (the scan angle in the cross-track direction). Our computer code transforms from global to antenna coordinates when evaluating g^2; equations for transforming between rotated coordinate systems are straightforward and can be found in many references, e.g., [8].

The surface σ^o is modeled as a function which decreases linearly with look angle θ in the log-domain and is independent of ϕ. σ^o is given by

$$\sigma^o(\theta) = \sigma^o(0^\circ) - \beta\theta \tag{12}$$

where $\sigma^o(0^\circ)$ and β are chosen to model either an ocean surface or a land surface. Both σ^o and $\sigma^o(0^\circ)$ are in decibels. In spite of its simplicity this model is similar to measurements of σ^o [9], [10]. For modeling an ocean surface, the parameters in our model are adjusted to provide an approximate match between the model σ^o and the measurements of σ^o in [9] for a wind speed of 7 m/s. In this case, $\sigma^o(0^\circ)$ is 12 dB and β is 0.7 dB per degree. For the land case, $\sigma^o(0^\circ)$ is chosen to be 0 dB and β is 0.2 dB per degree, providing an approximate match to experimental data [10].

Atmospheric attenuation depends on both atmospheric gases and presence of clouds and rain. While clouds and rain can cause large attenuations, their presence and location over the earth appear random. For the calculations in the following section, we assume that the attenuations for both the atmospheric and clutter returns are equal ($L_a = L_s$) and so cancel in the calculation of SCR. For specific meteorological situations, realistic values of L_a and L_s can be calculated and used in (10) (see [2]).

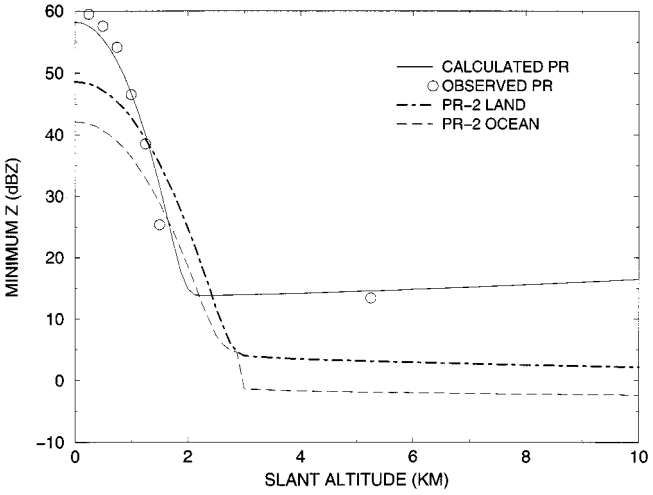

Fig. 2. Calculated Z_m at 17° due to clutter for TRMM PR (solid) and observed Z_m over the Indian Ocean (circles). Also shown is calculated Z_m at 37° scan angle for PR-2 over land (dot-dashed) and over ocean (dashed). Slant altitude is distance from surface to atmospheric target along radar look direction.

The scatterer velocity (relative to the radar) is a function of both the motion of the spacecraft and earth rotation. For these calculations, we assume a spacecraft in a circular orbit around a spherical earth, positioned over the equator and moving in a direction ψ, measured clockwise from the east (e.g., northward motion is $\psi = 90^\circ$). The total velocity of the surface is the sum of the spacecraft and earth rotation velocities. For the cross-track scan geometry analyzed here, only the earth's rotation contributes to the Doppler weighting for the atmosphere w_a, so w_a is always close to unity. To calculate the effect of the Doppler velocity, we need an explicit formula for the receiver transfer function. Here, we assume that $H(f)$ is a Gaussian, as done in [5] and [7].

III. Application to Radar Analysis and Design

The precipitation radar (PR) on the tropical rainfall measuring mission (TRMM) [11] is the first spaceborne atmospheric radar. Table I summarizes the PR performance characteristics; the antenna parameters were chosen to provide a pattern similar to the TRMM PR pattern [11]. Fig. 2 shows clear-air reflectivity versus slant altitude acquired by the TRMM PR over the Indian ocean for a scan angle α of 17°. Slant altitude is the distance along the radar look direction from the surface. In the TRMM PR processing, data below the thermal noise level are set to a flag which indicates that no signal is present. The points shown in Fig. 2 (as circles) are the only ones with valid data. Since the data are above the thermal noise and since conditions were clear (verified by TRMM imager data), the circles in Fig. 2 are interpreted as clutter. Also shown in Fig. 2 are calculations of Z_m due to clutter using the method developed in the previous section. The calculated clutter contribution to atmospheric targets from just above the surface to a slant altitude of about 15 km is dominated by

TABLE I
RADAR SYSTEM CHARACTERISTICS

Parameter	PR	PR-2	CPR
Frequency (GHz)	13.8	13.4	94
Altitude (km)	350	400	705
Max scan angle (^{o})	17	37	0
Horizontal resolution (km)	4	2	1.4
Range resolution (m)	250	250	500
PRF (Hz)	2776	2800	4200
Antenna diameter (m)	2.0	5.3	1.85
Antenna g_s	29	25	50
Antenna c	1.5	4.0	0.0
Receiver bandwidth (MHz)	0.6	4.0	0.3
Motion direction ψ (^{o})	35	70	98

same-pulse clutter (i.e., $n = 0$). At slant altitudes greater than 15 km, the range to the atmosphere is smaller than the radar altitude and only pulses with $n \geq 1$ can contribute. As the look angle decreases, the maximum slant altitude at which the $n = 0$ pulse contributes also decreases. At nadir the $n = 0$ pulse does not contribute to range bins above the surface. In this case the methods developed in [1]–[3] would predict no clutter. Using our method, we find that Z_m at nadir is -4 dBZ near the surface and increases to 0 dBZ at 15 km altitude. These values are well below the TRMM PR thermal noise, and, hence, are not a concern for TRMM PR data.

Because of the TRMM PRs success, a second-generation spaceborne precipitation radar (PR-2) is being investigated [12]. One of the goals of the new radar is to provide a sensitivity several decibels better than that of the TRMM PR. Hence, clutter is a concern. To design an antenna with acceptable performance, clutter calculations were performed for a variety of antenna patterns. Results from these calculations, along with other system considerations, were used in developing antenna requirements. Fig. 2 shows Z_m for the PR-2 due to clutter for the PR-2 parameters in Table I, using the maximum planned scan angle α of 37°. Both land and ocean results are shown. For slant altitudes below 2.9 km, the first contributing pulse is the $n = -2$ pulse. For slant altitudes greater than 2.9 km, the $n = -2$ pulse cannot contribute, resulting in a sudden drop in clutter for the ocean case at 2.9 km, visible in Fig. 2. Such a drop cannot be seen for the land case, since land clutter is dominated by the $n = 0$ pulse both below and above 2.9 km. The dominance of the $n = 0$ pulse in the land case is due to land's slower decrease in backscatter with look angle. Calculations were also made for PR-2 at nadir ($\alpha = 0°$). In this case, only pulses with $n \geq 1$ can contribute to range bins above the surface. As was the case for the PR, we find that for the PR-2 the $n \geq 1$ contribution at nadir is well below that of thermal noise, on the order of -10 dBZ for both land and ocean. This level is somewhat lower than for the TRMM PR due to a faster rolloff in sidelobes for the planned PR-2 antenna pattern (see Table I).

In addition to measuring precipitation, spaceborne radars are planned for cloud measurements. The utility of such systems is already being studied [13], and NASA plans to launch the CloudSat mission, which will carry a 94 GHz radar for cloud studies. Table I shows the expected cloud profiling radar (CPR) performance characteristics for CloudSat. Since CPR operates only at nadir, only pulses with $n \geq 1$ can contribute to range bins above the surface. Fig. 3 shows the calculated Z_m for land and ocean for CPR (the two upper curves). The minimum detectable reflectivity is well below the required -26 dBZ level. The 50 dB antenna sidelobes assumed here can be difficult to achieve. Such levels, however, are expected for the CPR antenna, which is an offset design to minimize sidelobes due to aperture blockage.

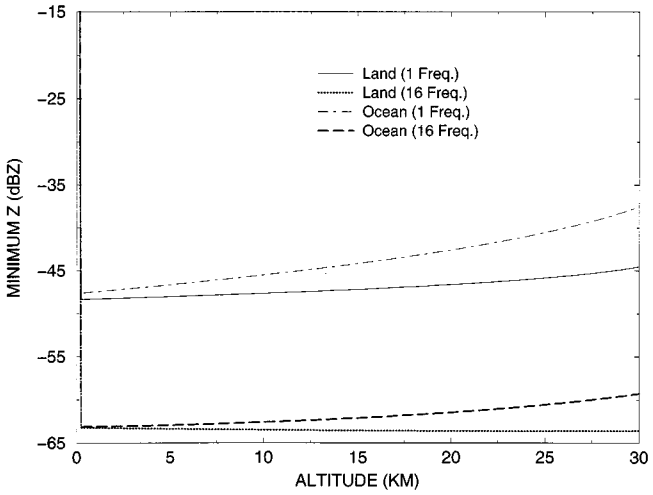

Fig. 3. Calculated Z_m at nadir for 94 GHz cloud profiling radar (CPR) with single frequency (upper two curves) and with frequency diversity using 16 frequencies (lower two curves), for land and ocean surfaces.

A method for achieving the required minimum reflectivity with poorer antenna sidelobe performance was also considered. Frequency diversity has previously been suggested as an approach for increasing independent samples [5]. Here, we consider frequency diversity as a method for suppressing range ambiguities. Specifically, the radar transmits a sequence of frequencies, changing the frequency for each pulse. The receiver tracks the transmit frequency with a delay corresponding to the pulse roundtrip time. At a given instant, the clutter from most previous pulses is outside the receiver passband. This is analogous to use of polarization diversity, first suggested in [14]. While it allows higher antenna sidelobes, this method does require more complicated electronics and is not used for CloudSat. It is, however, an option for future missions and is investigated here.

Fig. 3 shows results for a system with the CPR parameters in Table I but using a total of 16 transmit frequencies with 2 MHz spacing between each frequency. The sequence steps from lowest to highest frequency, and it is assumed that the first frequency in the sequence illuminates the atmosphere. It can be seen that frequency diversity provides a large reduction in clutter in both land and ocean cases. In fact, the CloudSat requirements could have been met using frequency diversity and an antenna with sidelobes near -40 dB. Fig. 4 shows the contribution of each annulus to the received clutter at 25 km altitude, both without and with frequency diversity. The first annulus occurs at $\theta = 9°$ and the last near 64°. The two-sided Doppler bandwidth of the first annulus is about 1.5 MHz. The width quickly increases to about 4 MHz at 25° (third annulus), 6 MHz at 40°, and 8 MHz at 60°. For the case without frequency diversity, the Doppler spectra of all annuli are centered on the receiver passband. When frequency diversity is used, the annuli have center frequencies shifted by 2–30 MHz. The first

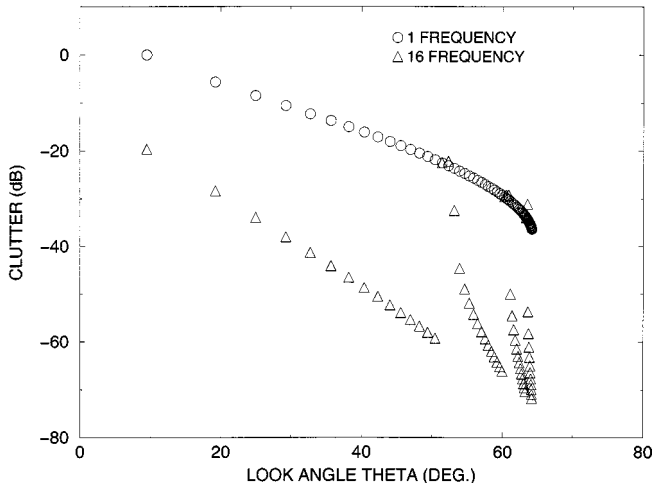

Fig. 4. Calculated normalized clutter contribution for each annulus for a CPR range bin at 25 km altitude for a land surface. Calculations without frequency diversity (circles) and with frequency diversity (triangles) are shown. Clutter in both cases is normalized by clutter from the first annulus for the single frequency case.

15 annuli have much smaller contributions in the frequency diversity case because they have center frequencies shifted away from the receiver passband. Even so, their contribution is not zero because of the presence of frequency domain sidelobes for the transmitted rectangular pulse and the receiver filter response. This is reflected in the weighting function $w(f_d)$, which is small but not identically zero for Doppler shifts much greater than the receiver bandwidth. Annuli for pulse 16 and its multiples have the same contribution with and without frequency diversity; these pulses use the same frequency as that illuminating the atmosphere in both cases.

IV. Conclusions

We have developed a method for calculating the surface return through antenna sidelobes for downward-looking atmospheric radar. The method is used to determine the minimum detectable reflectivity factor Z_m. It calculates clutter due not only to the same pulse as that illuminating the atmosphere but also all previous and subsequent pulses that can cause clutter return to occur simultaneously with the atmospheric return. The clutter calculation method presented here also includes the effect of Doppler shifting and finite receiver bandwidth and effect of a curved earth's surface.

The method was applied to existing and planned spaceborne radars. Calculations for the TRMM PR are in reasonable agreement with observations. For the TRMM PR same-pulse clutter is significant at lower altitudes when the antenna is scanned to large angles. Clutter is also present when the antenna is pointed at nadir, due to previously transmitted pulses. However, the clutter contribution at nadir is well below the thermal noise and is not observed. A planned second-generation precipitation radar (PR-2) was described, and the method developed here was used to simulate its performance and to verify the acceptability of the planned antenna pattern. Finally, for a cloud radar it was found that the weak return from clouds can easily be obscured by clutter. Use of very low antenna sidelobes or frequency diversity is needed to reduce the clutter to acceptable levels. As a result of these calculations, an antenna with very low sidelobes has been designed for the CloudSat CPR. Calculations presented here show that the clutter level should meet requirements.

References

[1] T. Manabe and T. Ihara, "A feasibility study of rain radar for the tropical rainfall measuring mission, 5. Effects of surface clutter on rain measurements from satellite," *J. Commun. Res. Lab.*, vol. 35, no. 145, pp. 163–181, 1988.

[2] R. Meneghini and T. Kozu, *Spaceborne Weather Radar*. Norwood, MA: Artech House, 1990.

[3] H. Hanado and T. Ihara, "Evaluation of surface clutter for the design of the TRMM spaceborne radar," *IEEE Trans. Geosci. Remote Sensing*, vol. 30, pp. 444–453, May 1992.

[4] J. R. Probert-Jones, "The radar equation in meteorology," *Q. J. R. Meteorol. Soc.*, vol. 88, pp. 485–495, 1962.

[5] R. J. Doviak and D. S. Zrnic, *Doppler Radar and Weather Observations*. New York: Academic, 1984.

[6] G. W. Stimson, *Introduction to Airborne Radar*: Hughes, 1984.

[7] R. J. Doviak and D. S. Zrnic, "Receiver bandwidth effect on reflectivity and Doppler velocity estimates," *J. Appl. Meteorol.*, vol. 18, pp. 69–76, 1979.

[8] L. Tsang, J. A. Kong, and R. T. Shin, *Theory of Microwave Remote Sensing*. New York: Wiley, 1985.

[9] L. C. Schroeder, P. R. Schaffner, J. L. Mitchell, and W. L. Jones, "AAFE RADSCAT 13.9 GHz measurements and analysis: Wind-speed signature of the ocean," *IEEE J. Oceanic Eng.*, vol. OE-10, pp. 346–357, 1985.

[10] F. T. Ulaby and M. C. Dobson, *Handbook of Radar Scattering Statistics for Terrain*. Norwood, MA: Artech House, 1989.

[11] C. Kummerow, W. Barnes, T. Kozu, J. Shiue, and J. Simpson, "The Tropical Rainfall Measuring Mission (TRMM) sensor package," *J. Atmos. Ocean. Technol.*, vol. 15, pp. 809–817, 1998.

[12] E. Im, S. L. Durden, G. Sadowy, A. Berkun, J. Huang, M. Lou, B. Lopez, Y. Rahmat-Samii, and S. Rengarajan, "System concept for the next-generation spaceborne precipitation radars," in *Proc. IEEE Aerospace Conf.*, Mar. 18–25, 2000.

[13] A. Guyot, J. Testud, and T. P. Ackerman, "Determination of the radiative properties of stratiform clouds from a nadir-looking 95-GHz radar," *J. Atmos. Ocean. Technol.*, vol. 17, pp. 38–50, 2000.

[14] R. J. Doviak and D. Sirmans, "Doppler radar with polarization diversity," *J. Atmos. Sci.*, vol. 30, pp. 737–738, 1973.

Stephen L. Durden (S'82–M'86–SM'99) received the B.S. degree in electrical engineering and applied mathematics from Rice University, Houston, TX, in 1980, and the M.S. and Ph.D. degrees in electrical engineering from Stanford University, Stanford, CA, in 1983 and 1986, respectively.

In 1986, he joined the Jet Propulsion Laboratory (JPL), California Institute of Technology, Pasadena, where he has worked on the NSCAT scatterometer project, the airborne polarimetric SAR program (AIRSAR), the airborne rain mapping radar (ARMAR), the airborne cloud radar, LightSAR, second-generation precipitation radar, CloudSat, and various research tasks involving modeling and analysis of radar observations of the ocean, land, and atmosphere. His current work includes radar systems design, development, and testing, as well as analysis of airborne precipitation radar data acquired during tropical rainfall measuring mission (TRMM) field experiments.

Eastwood Im (S'81–M'85–SM'00) received the B.S., M.S., and Ph.D. degrees in electrical engineering from the University of Illinois, Urbana, in 1981, 1982, and 1985, respectively.

He has been with the Jet Propulsion Laboratory (JPL), California Institute of Technology, Pasadena, since 1986. His research interests are in the areas of spaceborne meteorological radar science and remote sensing, and advanced radar system studies. In particular, he has developed radar algorithms for the retrievals of precipitation intensity and surface topography, and the two-color laser altimetry algorithms for measuring surface pressure and tectonic motions. He has been involved in several design studies on spaceborne earth remote sensing radars, including precipitation radar, altimeter, and millimeter-wave cloud radar.

Currently, he is the Radar Manager of the NASA ESSP CloudSat mission and the Supervisor of the atmospheric radar science and engineering group at JPL. He has been a member of the tropical rainfall measuring mission (TRMM) science team in the areas of radar algorithms for rainfall profile retrieval and TRMM radar calibration. He is the Principal Investigator of the NASA IIP second-generation precipitation radar (PR-2) task. He has been a member of science steering group for the NASA global precipitation mission. He has published over 90 articles in refereed journals and conference proceedings. He is currently the Associate Editor of the AMS *Journal of Atmospheric and Oceanic Technology*.

Dr. Im is a member of the American Meteorological Society, Eta Kappa Nu, and Tau Beta Pi. He received the University of Illinois Graduate College Dissertation Research Grant in 1984, the GT&E Fellowship in 1984, the Kemper Fellowship in 1985, and the Exxon Fellowship in 1985.

Fuk K. Li (SM'89–F'96) received the B.Sc. and Ph.D. degrees in physics from the Massachusetts Institute of Technology, Cambridge, in 1975 and 1979, respectively.

He joined the Jet Propulsion Laboratory, California Institute of Technology, Pasadena, in 1979, and has been involved in various radar remote sensing activities. He has developed a number of system analysis tools for spaceborne synthetic aperture radar (SAR) system design, a digital SAR processor and simulator, investigated techniques for multilook processing and Doppler parameter estimations for spaceborne SARs, and evaluated the tradeoffs in SAR image parameters. He also participated in the development of system design concepts and applications for interferometric SAR. He was the Project Engineer for the NASA scatterometer and was responsible for the technical design of the system. He was the Principal Investigator for an airborne rain-mapping radar and was using data obtained from that system for rain retrieval algorithm development studies in support of the tropical rain measuring mission (TRMM). He was also a Principal Investigator for an experiment utilizing the SIR-C/X-SAR systems to study rainfall effects on ocean roughness and rain retrieval with multiparameter SAR observations from space. He is also leading the development of an airborne cloud profiling radar (CPR) and the development of an active/passive microwave sensor for ocean salinity and soil moisture sensing. He is currently Manager of the New Millennium Program.

Ralph Girard received the B.Sc. degree in physics and the M.Sc. and Ph.D. degrees in theoretical physics from Laval University, Quebec, QC, Canada, in 1981, 1983, and 1987, respectively.

From 1988 to 1991, he was an NRC Postdoctoral Fellow with the Max Planck Institut für Kernphysik, Heidelberg, Germany, and with the University of Montreal, Montreal, QC, working on computational physics applications in field theory and quantum chromodynamics. In 1991, he became an NRC Industrial Research Fellow at MPB Technologies, Pointe-Claire, QC, Canada, working on applied electromagnetics and spaceborne radar remote sensing applications. In 1999, he joined the Space Technologies division of the Canadian Space Agency, St. Hubert, QC, working on SAR and radar for atmospheric remote sensing. His current work centers on development of technology and applications for spaceborne radars.

Kyung S. Pak received the B.S. degree in physics and the M.S. and Ph.D. degrees in electrical engineering from the University of Washington, Seattle, in 1990, 1992, and 1996, respectively.

He has been with the Radar Science and Engineering Section, Jet Propulsion Laboratory, California Institute of Technology, Pasadena, since 1996. He is engaged in the study of spaceborne microwave and millimeter-wave radar performance, calibration, and science data processing. His research interests include electromagnetic wave scattering from rough surfaces and remote sensing of the ocean and atmosphere.